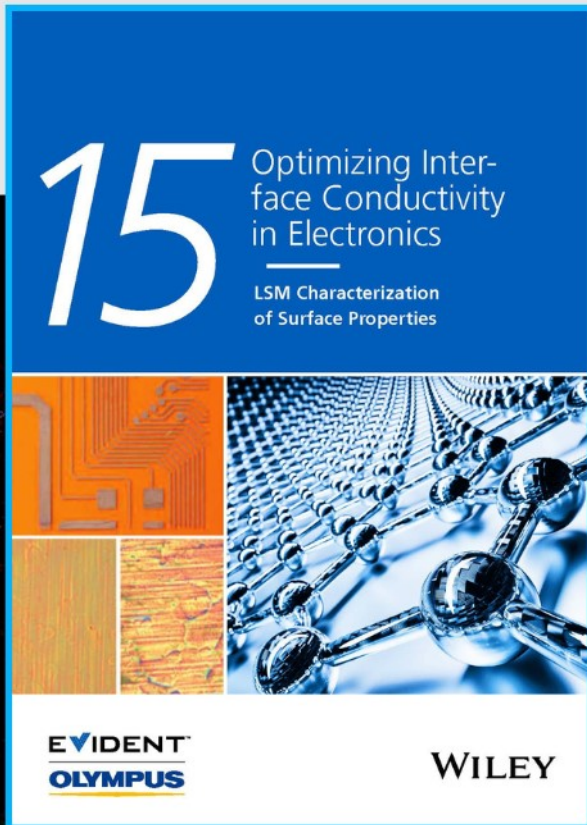




Optimizing Interface Conductivity in Electronics



The latest eBook from
Advanced Optical Metrology.
Download for free.

Surface roughness is a key parameter for judging the performance of a given material's surface quality for its electronic application. A powerful tool to measure surface roughness is 3D laser scanning confocal microscopy (LSM), which will allow you to assess roughness and compare production and finishing methods, and improve these methods based on mathematical models.

Focus on creating high-conductivity electronic devices with minimal power loss using laser scanning microscopy is an effective tool to discern a variety of roughness parameters.

EVIDENT
OLYMPUS

WILEY

Direct Growth of Nanopatterned Graphene on Sapphire and Its Application in Light Emitting Diodes

Zhaolong Chen, Hongliang Chang, Ting Cheng, Tongbo Wei,* Ruoyu Wang, Shen Yuan Yang, Zhipeng Dou, Bingyao Liu, Shishu Zhang, Yadian Xie, Zhiqiang Liu, Yanfeng Zhang, Jinmin Li, Feng Ding,* Peng Gao,* and Zhongfan Liu*

Direct growth of graphene films on functional substrates is immensely beneficial for the large-scale applications of graphene by avoiding the transfer-induced issues. Notably, the selective growth of patterned graphene will further boost the development of graphene-based devices. Here, the direct growth of patterned graphene on the *c*-plane of nanopatterned sapphire substrate (NPSS) is realized and the superiority of the patterned graphene for high-performance ultraviolet light-emitting diodes (UV-LED) is demonstrated. As confirmed by density functional theory calculations and analog simulations, compared to the concave *r*-plane the flat *c*-plane of NPSS is characterized by a lower active barrier for methane decomposition and carbon species diffusion, as well as a greater supply of carbon precursor for graphene growth. The synthesized patterned graphene on the *c*-plane of NPSS is verified to be monolayer and high quality. The patterned graphene enables the selective and well-aligned nucleation of aluminium nitride (AlN) to promote rapid epitaxial lateral overgrowth of single-crystal AlN films with low dislocation density. Consequently, the fabricated UV-LED demonstrates high luminescence intensity and stability. The method is suitable for obtaining various patterned graphene by substrate design, which will allow for greater progress in the cutting-edge applications of graphene.

1. Introduction

Graphene is the focus of extensive research efforts worldwide due to its fascinating physical properties,^[1,2] such as ultrahigh electrical^[3] and thermal conductivity,^[4] good mechanical strength, and excellent elasticity,^[5] among others.^[6–9] Moreover, graphene maintains excellent stability in the presence of extremely high temperatures and harsh chemical environments. These superior properties make graphene a promising material for myriad applications in electronics,^[7,8,10] optoelectronics,^[11] energy generation and storage,^[12] and biosensor.^[13] Among graphene synthesis methods, chemical vapor deposition (CVD) possesses unique advantages compared to various traditional methods. CVD synthesis of large-area and high-quality graphene films is usually performed on metal foils, such as Ni^[14] or Cu.^[15] However, this is not compatible with standard semiconductor

Dr. Z. L. Chen, T. Cheng, R. Y. Wang, S. S. Zhang, Y. D. Xie, Prof. Y. F. Zhang, Prof. Z. F. Liu
Center for Nanochemistry (CNC)
Beijing Science and Engineering Center for Nanocarbons
Beijing National Laboratory for Molecular Sciences
College of Chemistry and Molecular Engineering
Peking University
Beijing 100871, China
E-mail: zfliu@pku.edu.cn

Dr. Z. L. Chen, T. Cheng, R. Y. Wang, Y. D. Xie, Prof. Y. F. Zhang, Prof. Z. F. Liu
Beijing Graphene Institute (BGI)
Beijing 100095, China

H. L. Chang, Prof. T. B. Wei, Prof. Z. Q. Liu, Prof. J. M. Li
State Key Laboratory of Solid-State Lighting
Institute of Semiconductors
Chinese Academy of Sciences
Beijing 100083, China
E-mail: tbwei@semi.ac.cn

H. L. Chang, Prof. T. B. Wei, Prof. S. Y. Yang, Prof. Z. Q. Liu, Prof. J. M. Li
Center of Materials Science and Optoelectronics Engineering
University of Chinese Academy of Science
Beijing 100049, China

T. Cheng, B. Y. Liu
Academy for Advanced Interdisciplinary Studies
Peking University
Beijing 100871, China

Prof. S. Y. Yang
State Key Laboratory of Superlattices and Microstructures
Institute of Semiconductors
Chinese Academy of Sciences
Beijing 100083, China

Z. P. Dou, B. Y. Liu, Prof. P. Gao
Electron Microscopy Laboratory, and International Center for Quantum Materials
School of Physics
Peking University
Beijing 100871, China
E-mail: p-gao@pku.edu.cn

 The ORCID identification number(s) for the author(s) of this article can be found under <https://doi.org/10.1002/adfm.202001483>.

DOI: 10.1002/adfm.202001483

manufacturing process by involving the subsequent complex transfer procedure.^[16,17] Furthermore, for most of applications, patterned graphene film is highly desirable,^[18–20] in which case multiple processing steps are inevitable, including photo/e-beam lithography, and wet/dry etching. These processes are high-cost and, more importantly, leads to a deterioration in graphene quality by introducing uncontrollable breakages, wrinkles, and contamination, resulting a low yield. Therefore, there is great motivation to realize the direct growth of patterned graphene on dielectric substrates.

Up to now, some progress have been made on direct growth of graphene on dielectric substrates (sapphire, SiO₂/Si, Si₃N₄, quartz, etc.) by using metal-free CVD method.^[21,22] Among these substrates, sapphire (aluminum oxide, α -Al₂O₃) is widely used for growth of single crystal metal,^[23,24] high-temperature superconductors,^[25,26] and semiconductor films,^[27,28] as well as for integrated circuit fabrication. Graphene/sapphire hybrids show highly valuable applications in electronics (e.g., field effect transistors) due to the advantages imparted by the relatively high *k* of α -Al₂O₃ as a gate insulator.^[29,30] Moreover, graphene buffered sapphire, have been demonstrated as ideal ways for achieving van der Waals epitaxy of Group-III nitride films for high-performance light-emitting diodes.^[31,32] The direct growth of patterned graphene on sapphire would further boost these cutting-edge applications of graphene in semiconductor and electronic industry. However, to our knowledge, the direct growth of patterned graphene remains underexploited and thus, urgently need to be solved.

Here, we demonstrate the direct growth of nanopatterned, high-quality, monolayer graphene by selectively growing on *c*-plane of nanopatterned sapphire substrate (NPSS) and show their application in superior epitaxy of aluminium nitride (AlN) film. The nanoconcave triangle cones patterns of NPSS lead to that the gas velocity at concave *r*-plane is nearly two orders of magnitude slower than that at the flat *c*-plane (according to 2D qualitative simulation). Furthermore, density functional theory (DFT) calculation reveals relatively lower energy barriers for methane dissociation and active carbon species diffusion on the *c*-plane compared to the *r*-plane. The combined effects of a sufficient supply of carbon precursor and relatively low dissociation and diffusion barriers on the flat *c*-plane make possible the selective growth of graphene. During the subsequent AlN growth process, we find that the patterned graphene enables the selective and well-aligned nucleation of AlN to promote

rapid epitaxial lateral overgrowth (ELOG) of single-crystal AlN films with low dislocation density even without low temperature AlN buffer layer. Consequently, the fabricated ultraviolet light-emitting diodes (UV-LED) demonstrate high luminescence (EL) intensity and stability. The insights granted by this study to indicate great opportunity to adjust the pattern structure (i.e., nanoribbons for field effect transistor) of graphene by designing the pattern of sapphire substrate.

2. Results and Discussion

2.1. Selective Growth of Graphene on *c*-Plane of NPSS

As illustrated in **Figure 1a**, we used the direct metal-free CVD method to realize the selective growth of graphene on *c*-plane of NPSS. In this study, the NPSS was acquired via nanosphere lithography assisted anisotropic etching of (0001) *c*-oriented sapphire.^[33] Atomic force microscopy (AFM) image of the fabricated NPSS revealed surface patterns of concave triangle cones which exhibited a periodicity of $\approx 1\ \mu\text{m}$ and a depth of $\approx 230\ \text{nm}$. The side faces of each triangle cone were three facets of the (1 $\bar{1}$ 02) *r*-plane with an angle of 57° against the (0001) *c*-axis (**Figure 1b**).^[34] After the CVD process, graphene selectively covered the flat *c*-plane, as indicated by a brighter contrast compared to the concave *r*-plane in the scanning electron microscopy (SEM) image (**Figure 1c**). Raman spectra and mapping in **Figure 1d** further confirmed the successfully growth of patterned graphene, as evidenced by a relatively strong Raman signal of graphene observed on the *c*-plane and a negligible signal on the *r*-plane. These results indicate key differences between the growth behavior of graphene on the *c*-plane and *r*-plane, namely that carbon species tend to preferentially nucleate and grow on the *c*-plane.

2.2. Characterization of the As-Grown Patterned Graphene on *c*-Plane of NPSS

No characteristic signals of transition metal elements appears in the full range X-ray photoelectron spectroscopy (XPS) spectrum (**Figure 2a**) due to the metal-free CVD growth technique. Thus, the lack of metal pollutants meets the requirement of semiconductor manufacturing process. The C 1s XPS spectrum of the as-grown graphene patterned exhibits a dominant sp²-carbon-related peak (284.8 eV), a C–H related peak (285.4 eV), and broad C–O related peaks (**Figure 2b**), indicating its high quality. The low D band in the Raman spectrum (**Figure 1d**) along with a correspondingly a low *I_D*/*I_G* intensity ratio (≈ 0.7), also conforms the high quality of as-grown patterned graphene. After transfer to a copper grid, the selectively grown graphene was further assessed for its thickness and crystallinity via transmission electron microscopy (TEM). We find the graphene film was predominantly monolayer according to the image of film breakage edges (**Figure 2c**). Moreover, we use high-angle annular dark-field scanning transmission electron microscopy imaging mode of Cs-TEM to reveal the quality of as-grown patterned graphene at atomic scale which reveals the perfect atomic lattice of monolayer graphene (**Figure 2d**). This is also consistent with Raman and XPS results.

Prof. F. Ding
Centre for Multidimensional Carbon Materials
Institute for Basic Science
Ulsan 44919, Republic of Korea
E-mail: f.ding@unist.ac.kr

Prof. F. Ding
School of Materials Science and Engineering
Ulsan National Institute of Science and Technology
Ulsan 44919, Republic of Korea

Prof. P. Gao
Collaborative Innovation Center of Quantum Matter
Beijing 100871, China

Prof. P. Gao
Beijing Key Laboratory of Quantum Devices
Beijing 100871, China

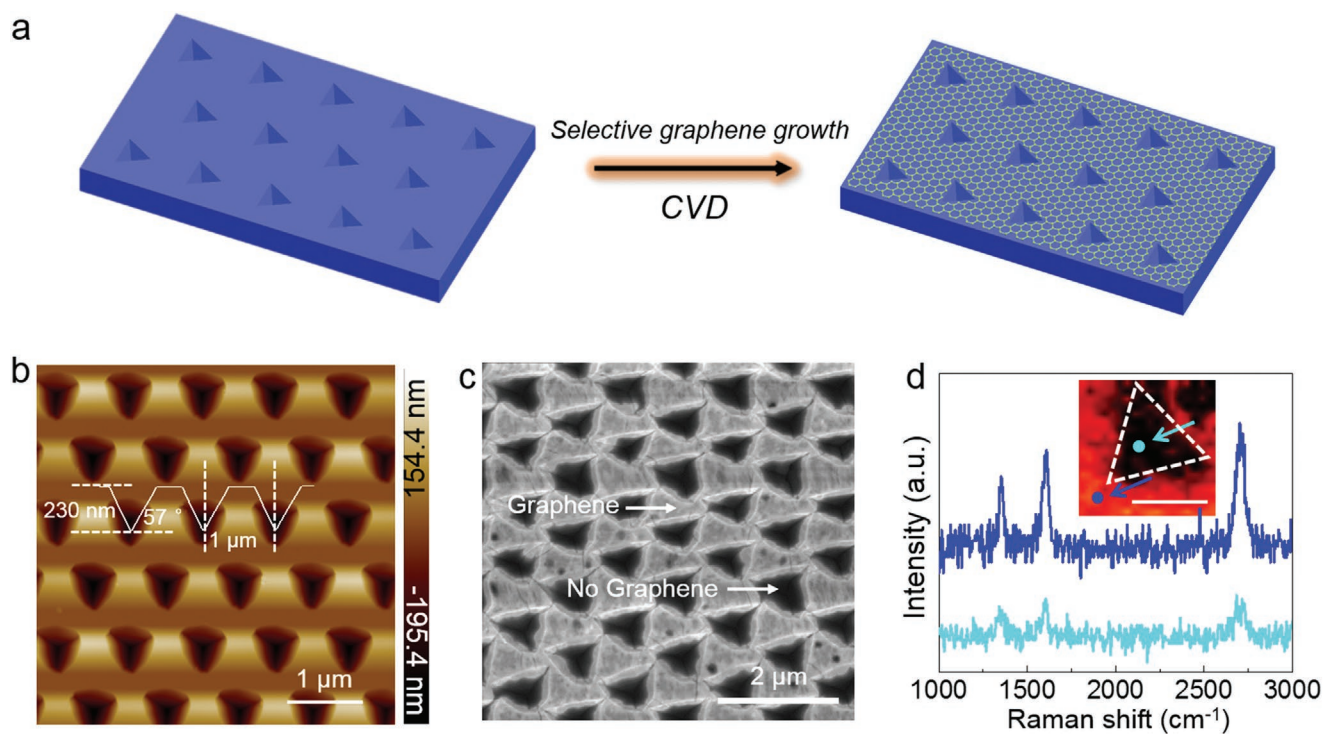


Figure 1. Selective growth of graphene on *c*-plane of NPSS. a) Schematic diagram of the selective growth of graphene on *c*-plane of NPSS. b) AFM height image of NPSS surface with concave triangle cones. c) SEM image of the as-grown patterned graphene on NPSS. d) Typical Raman spectra of selectively grown (patterned) graphene on the flat *c*-plane and concave *r*-plane of NPSS. Inset shows the Raman mapping of one pattern of selectively grown graphene on NPSS. Scale bar: 1 μm .

2.3. DFT Calculation for the Selective Growth of Graphene

To understand the phenomenon of selective graphene growth on *c*-plane of NPSS, we systematically studied the main dehydrogenation process of methane on the possible stable surface of *c*-plane and *r*-plane sapphire by first-principle calculations from atomic perspective. Different from the copper substrate, sapphire exhibits more diverse and complicated surface structures due to its binary elemental composition (several different possible surface configurations were constructed in Figures S1 and S2, Supporting Information), which strongly related with environmental chemical potential. Figure 3a displays the DFT-calculated surface energy per area of *c*-plane sapphire as a function of O chemical potential (The detailed chemical potential related surface energy for *c*-plane and *r*-plane sapphire are shown in Figure S3, Supporting Information). According to the calculated surface energy per area and suitable chemical potential interval (green shaded bar in Figure 3a) corresponding to our experimental conditions, we could finally obtain the geometries for the most stable surfaces of *c*-plane and *r*-plane sapphire, which are shown in Figure 3b,c (Similar stable surface structures have also been discussed in previous literature^[35,36]).

Based on these calculated stable *c*-plane and *r*-plane surface models, we further investigated the kinetics of CH_4 dissociation (Figure 3d). Owing to the inert properties of the sapphire surface, the dissociation of methane on both *c*-plane and *r*-plane sapphire is endothermic and marked by a high activation energy barrier compared to the analogous process on catalytic

metal substrate. The rate limiting step of the decomposition chain reaction is expected to be the first step, $\text{CH}_4 \rightarrow \text{CH}_3 + \text{H}$, as its product is a reactant in the subsequent step, $\text{CH}_3 + \text{H} \rightarrow \text{CH}_2 + \text{H}_2$. The activation barrier of the first reaction step on the *c*-plane was calculated to be 1.04 eV, which is much lower than that on the *r*-plane (1.61 eV), indicating that CH_4 decomposition on the *c*-plane could be expected $(0.57 \text{ eV/kT}) \approx 400$ times faster than that on the *r*-plane at the growth temperature of 1050 $^\circ\text{C}$ (Figure 3d). Therefore, *c*-plane sapphire is much more enriched with active carbon species than *r*-plane sapphire, and consequently is much more favorable for graphene growth. Further calculations showed that the activation barriers of the second decomposition step on *c*-plane and *r*-plane sapphire are relatively high at 3.61 and 3.93 eV, respectively, thereby resulting in very slow growth of graphene. As the calculated reaction energy of the first step of CH_4 decomposition on *c*-plane and *r*-plane sapphire is 0.11 and 0.59, respectively, and that of the second step is 2.53 and 2.22 eV, respectively, CH_2 is highly unstable on both surfaces. These calculations reveal that CH_2 concentration must be orders magnitudes lower than that of CH_3 whose radicals are the key species governing graphene growth on sapphire. The high instability and very low concentration of CH_2 on these surfaces render the following dehydrogenation steps negligible in determining graphene growth. To grow graphene requires the diffusion of decomposed radicals on the sapphire surface. The calculated diffusion barriers of CH_3 and CH_2 on both surfaces, which are shown in Figure 3e,f indicate that diffusion is much faster on the *c*-plane than on the *r*-plane. In

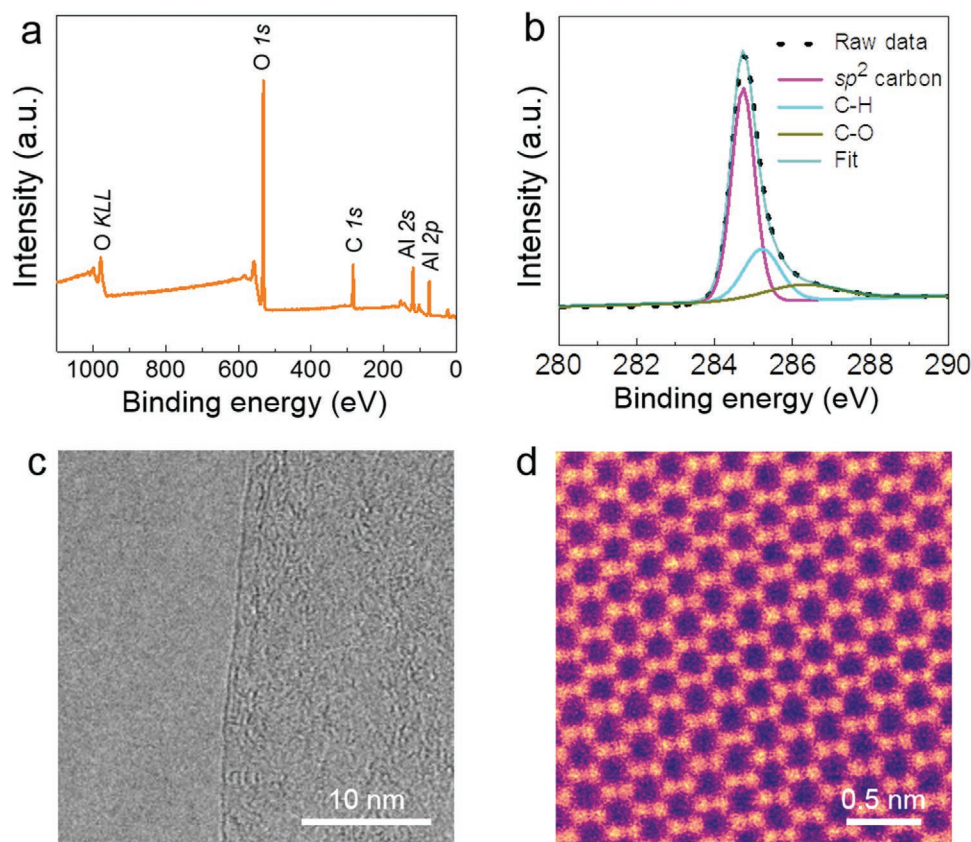


Figure 2. Characterization of the as-grown patterned graphene on *c*-plane of NPSS. a) Full range XPS spectrum of the as-grown patterned graphene on *c*-plane of NPSS. b) C 1s XPS spectrum of the as-grown patterned graphene on NPSS. c) Representative TEM image of the patterned graphene edge showing its monolayer structure. d) Atomically resolved image of patterned graphene which reveals its high crystallinity.

conclusion, the higher activity of *c*-plane sapphire compared to *r*-plane sapphire under the experimental conditions resulted in its enhanced abilities to facilitate CH₄ decomposition and radical diffusion, which contributed to the preferential growth of graphene on *c*-plane of NPSS.

2.4. The Controllable Growth of Graphene on NPSS

This DFT calculation demonstrates that the selective graphene growth is induced by the relatively reduced activity of the *r*-plane for methane decomposition. To confirm this, we also grow graphene on flat *c*-plane sapphire under the same growth condition. Graphene randomly nucleated and eventually form a continuous film on the flat *c*-plane sapphire (Figure S4a,b, Supporting Information). The Raman spectrum of graphene grown on flat *c*-plane sapphire shows relatively lower D band peak and higher 2D band peak (Figure S4c, Supporting Information), probably owing to the increased domain size and reduced edges. Furthermore, the 2D distribution of flow velocity around NPSS was simulated. The simulated carbon source distributions of flow velocity are depicted in **Figure 4a**, which clearly shows that the gas velocity is nearly two order of magnitude slower at the concave *r*-plane than that at the flat *c*-plane of NPSS. As a result, *c*-plane of NPSS is much more

enriched in carbon precursor. As such, graphene growth could be expected on both planes, if more active carbon species is supplied. To test this proposal, we performed graphene growth on NPSS using an ethanol feedstock under low pressure. The distribution of gas flow velocity around NPSS under low pressure was very uniform (Figure 4b). Moreover, ethanol is much easier to decompose than methane, even at a relatively low temperature.^[37] Therefore, a continuous graphene film is deposited on the concave *r*-plane and flat *c*-plane surfaces of NPSS, as confirmed by uniform contrast in SEM image (Figure 4c) and indiscriminate Raman spectra (Figure 4d).

2.5. Fabrication of UV-LED on Patterned Graphene/NPSS

NPSS is regarded as the most promising substrate to epitaxy AlN films and DUV-LEDs because it can yield significantly improved light extraction efficiency of LED.^[38,39] Moreover, it has been proposed that graphene can effectively overcome the effects of the large lattice and thermal mismatches between III-nitride and sapphire.^[30,31] Along this line, we find that potential energy from the sapphire substrate was well transmitted through monolayer graphene as shown in Figure S5 (Supporting Information), ensuring the growth of single-crystalline film. We directly grew AlN on the thus obtained patterned

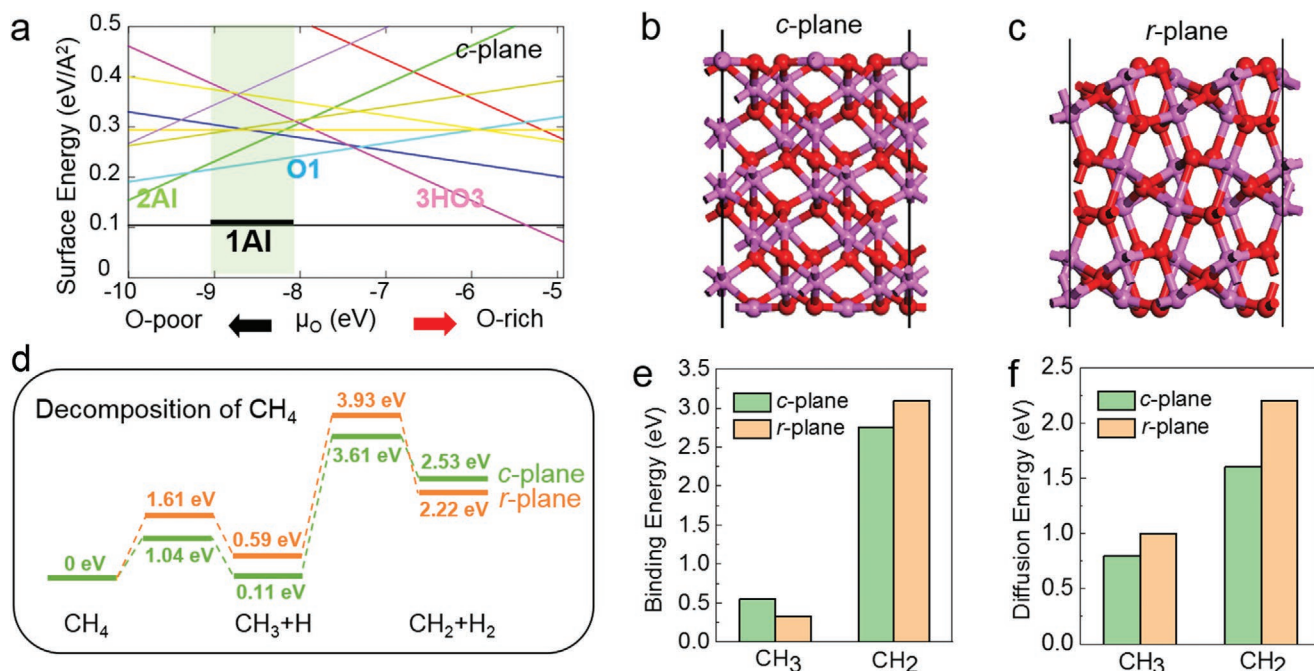


Figure 3. DFT calculation for the selective growth of graphene on *c*-plane of NPSS. a) DFT-calculated surface energy per area as a function of O chemical potential, with μ_H maintained at 1 eV for *c*-plane of sapphire. Different geometries, such as “1Al,” “2Al,” “O1,” and “3HO3,” (see Figures S1 and S2, Supporting Information) are depicted in different colors. The green shaded region is the corresponding chemical potential interval of the selected experimental condition. b,c) Side view of selected stable model of *c*-plane b) and *r*-plane c) sapphire, with oxygen and aluminum atoms represented in red and purple, respectively. d) Energy profiles of the dehydrogenation process of CH₄ at the surfaces of *c*-plane (green line) and *r*-plane (orange line) sapphire. e,f) Binding energy e) and diffusion barrier f) of CH₃ and CH₂ species on the surfaces of *c*-plane (green bars) and *r*-plane (orange bars) sapphire.

graphene/NPSS without low temperature buffer layer and nitrogen plasma treatment was applied to enhance graphene reactivity for AlN nucleation.^[31] As a result, AlN preferentially nucleated on the patterned graphene film atop *c*-plane of NPSS and the reduced diffusion barrier of adatoms on the graphene surface promoted ELOG of the AlN film. SEM image of the AlN after only 6 min of initial growth on patterned graphene/NPSS showed that AlN tended to nucleate and rapidly coalesce on plasma treated graphene, whereas negligible nucleus was observed on the bare concave *r*-plane of NPSS (Figure 5a). Increasing the growth time to 3 h, AlN grown on patterned graphene/NPSS have already covered the holes with continuous and smooth features (Figure 5b). Moreover, we can also observe the enhanced ELOG process induced by the patterned graphene by formation of air void and smooth surface (Figures S6–S9, Supporting Information). Such air void formation was negligible or absent in bare NPSS and full graphene covered NPSS (Figures S6–S9, Supporting Information), possibly due to the indiscriminate nucleation and growth of AlN on both *c*-plane and *r*-plane of NPSS. The dark field image of AlN grown on patterned graphene/NPSS with $g = 0002$ is shown in Figure 5c, wherein threading dislocations were observed to originate from the interface between AlN and graphene/NPSS, bend and finally annihilate around the voids, as confirmed by the largely reduced (10 $\bar{1}2$) full width at half maximum (FWHM) and (0002) FWHM (Figure 5d; and Figure S10, Supporting Information). Moreover, the large-scale view of electron backscatter diffraction mapping shows that the as-grown AlN epilayer was single-crystalline and exhibited (0001) orientation (Figure S11, Supporting

Information). Therefore, high quality AlN films can be directly grown on patterned graphene/NPSS without low temperature buffer layers, which would greatly shorten the metal organic CVD (MOCVD) growth time and thus reduce the cost.

UV-LED was further fabricated based on such high quality AlN films and the photograph is shown in Figure 5e. The EL characteristics of the UV-LED with and without patterned graphene depicted in Figure 5e demonstrate that under a current of 40 mA, the luminescence intensity with patterned graphene is nearly 3 times stronger than that of bare NPSS. The packaged LEDs with patterned graphene also shows a much enhanced light output power than that without graphene, which is consistent with EL spectra measured on wafer. At an injection current of 350 mA, the external quantum efficiency (EQE) of LED with patterned graphene is 10.84%, which is 90% higher than the device without patterned graphene (Figure S12, Supporting Information). Meanwhile, the presence of patterned graphene also alleviates the droop effect and the droop rate is decreased from 54.2% to 42.6%. The peak efficiency current density, I_{max} , at which the EQE shows the maximum value is also increased from 8 to 10 A cm⁻² with the assistance of patterned graphene. This strengthened luminescence mainly originated from the reduced defect density enabled by using patterned graphene as a buffer layer. The robustness of UV-LED was evaluated by adjusting the injection current across the range of 20–500 mA. Escalating the current from 20 to 100 mA initially caused the UV-LED without graphene blueshift from 385.9 to 383.6 nm due to band filling effect and a screening effect by the internal polarization electric field. Further increasing the current to 500 mA resulted in a

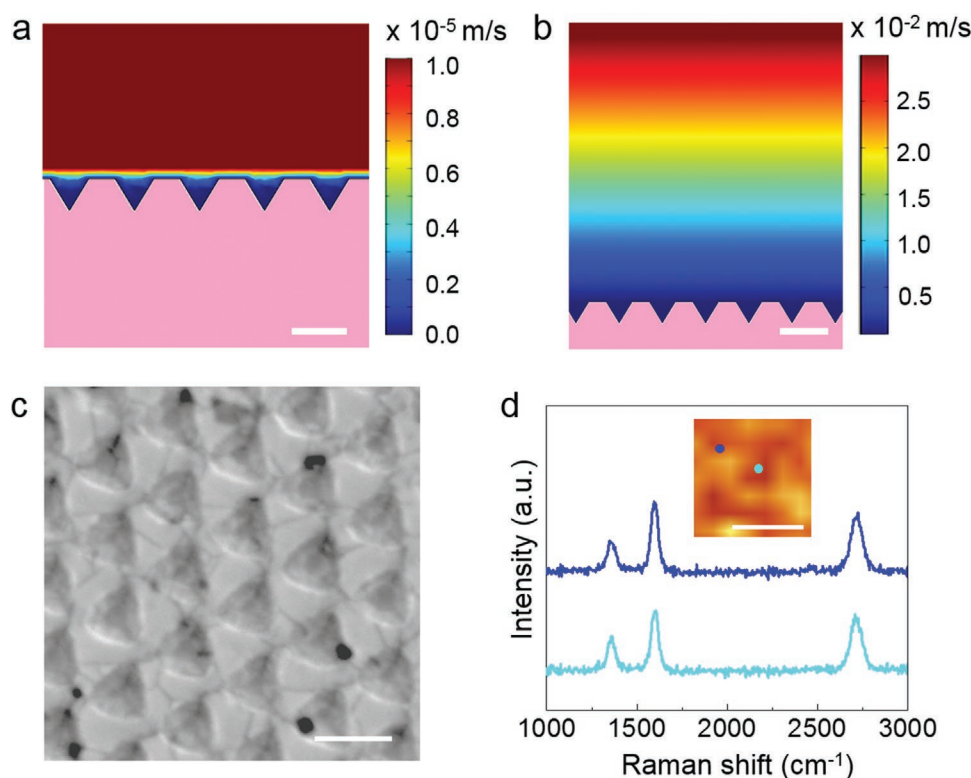


Figure 4. The controllable growth of graphene on NPSS by adjusting carbon precursor and system pressure. a) 2D simulated distributions of the gas velocity at the NPSS surface (atmospheric pressure, 100 sccm Ar, 50 sccm H₂, 15 sccm CH₄). b) 2D simulated distributions of the gas velocity at the NPSS (1500 Pa, 500 sccm Ar, 300 sccm H₂, 300 sccm ethanol). c) SEM image of the full graphene covered NPSS. d) Typical Raman spectra of full graphene covered NPSS. Inset shows the Raman mapping of full graphene covered NPSS. Sale bar: 1 μm.

redshift to 397.8.4 nm (Figure S13, Supporting Information), because a severe nonradiative recombination induces high thermal effect in poor crystal quality epilayer. The luminescence peak of UV-LED on patterned graphene/NPSS is located around 380 nm and negligible sensitivity to current, indicating significant stress relaxation and improved crystal quality facilitated by graphene (Figure 5f). Overall, the patterned graphene realizes the locationally controlled nucleation of AlN on desired locus and further enhances ELOG process with reduced dislocation density, targeting to high-performance UV-LEDs.

3. Conclusion

In summary, we have successfully achieved the direct growth of patterned graphene by utilizing physical design and chemical property of NPSS and realized their critical application in epitaxy of AlN film. DFT calculations and analog simulations confirmed that compared to the concave *r*-plane, the flat *c*-plane is characterized by lower active barriers for methane decomposition and active carbon species diffusion, as well as a greater supply of carbon precursor for graphene growth. Thus obtained patterned graphene on the flat *c*-plane of NPSS was verified to be monolayer and high quality. During subsequent AlN growth, the patterned graphene enhanced the ELOG process by promoting selective nucleation of AlN and reducing the diffusion barrier. Thus obtained AlN epilayer on “selectively” grown

graphene/NPSS exhibited substantially reduced dislocation density and, accordingly, high-performance UV-LED can be fabricated. Moreover, the growth of AlN on graphene/NPSS only requires one-step process without low temperature AlN buffer which can shorten the MOCVD growth time and cost. This work can motivate and inform further advancements, such as the controllable growth of various patterned graphene on dielectric substrates for electronic device applications, fulfilling the cutting-edge applications of graphene.

4. Experimental Section

Fabrication of NPSS: The NPSS which served as a substrate for this study was fabricated by the nanosphere lithography assisted wet etching method. In short, 200 nm thick SiO₂ film was deposited on *c*-sapphire and subsequently coated with positive photoresist and polystyrene (PS) nanospheres. Photolithography was conducted to remove PS nanospheres and then inductively coupled plasma etching of SiO₂ were applied. Finally, the sapphire was etched in a mixed solution (H₂SO₄:H₃PO₄ = 3:1) for 10 min, and the SiO₂ mask was removed by hydrofluoric acid.

Selective Growth of Graphene on Nanopatterned Sapphire Substrate: The fabricated NPSS was loaded into a high-temperature furnace. Then, the furnace was heated to 1050 °C, and maintained in air for 1 h. After replacing the air with Ar, introducing 150 sccm Ar, 50 sccm H₂, and 15 sccm CH₄ for the growth of graphene for about 3 h.

MOCVD Growth of AlN on Selectively Grown Graphene/NPSS: The selectively grown graphene/NPSS was treated by N₂ plasma at 50 W

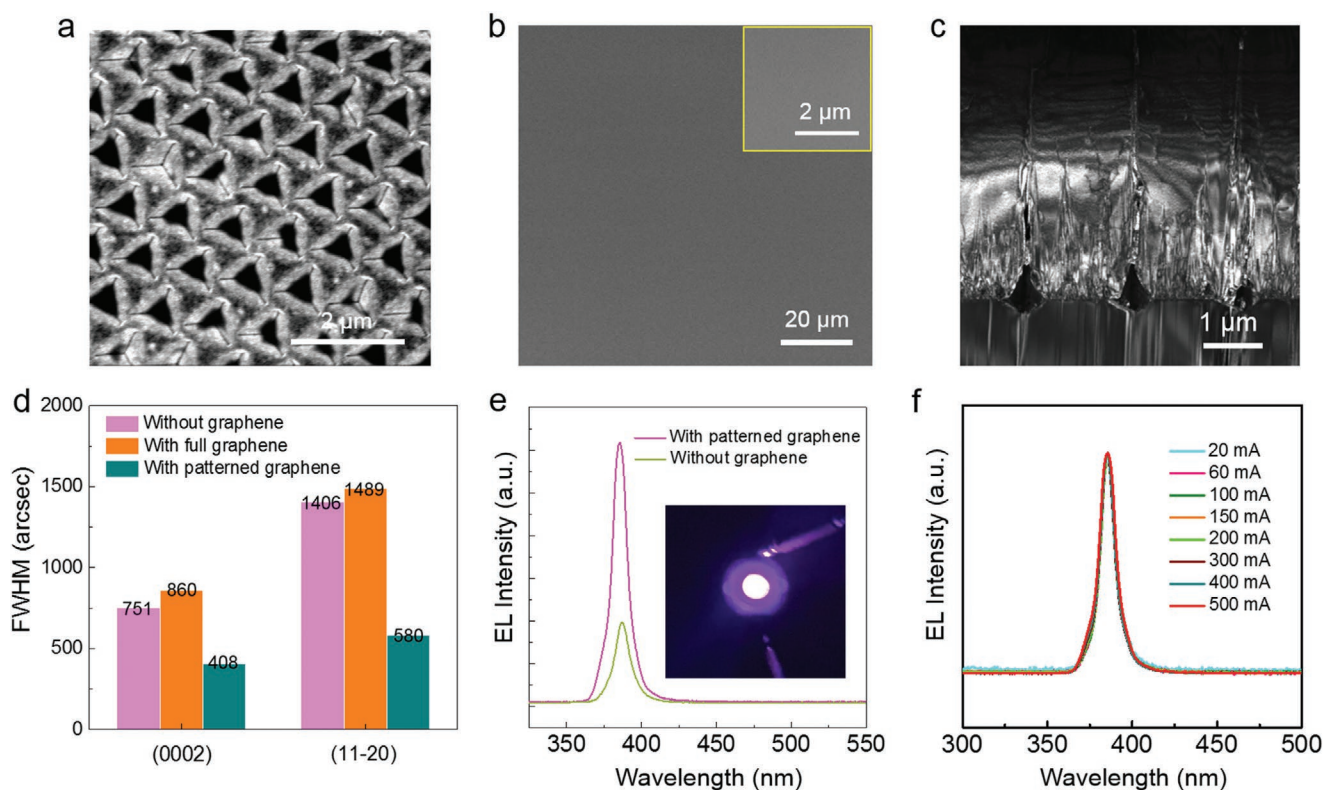


Figure 5. Patterned graphene enables fast growth of high quality AlN film on NPSS and high performance LED fabrication. a) SEM image of the initial growth of AlN on patterned graphene/NPSS (1200 °C, 500 sccm N₂, 50 sccm H₂, 15 ccm TMAI, 6 min). b) SEM images of as-grown AlN film on "selectively" grown graphene/NPSS after 3 h. c) Dark field image of as grown AlN film with $g = 0002$. d) Histogram of (10 $\bar{1}2$) FWHM and (0002) FWHM for AlN films grown on bare NPSS, full graphene covered NPSS, and patterned graphene covered NPSS. e) EL spectra of the UV-LED on NPSS with and without the patterned graphene under a current of 40 mA for on-wafer measurement. Inset is the photograph of the electroluminescence from the UV-LED with patterned graphene. f) The normalized EL spectra of UV-LED on patterned graphene/NPSS with inject current ranging from 20 to 500 mA.

power for 30 s before it was loaded into the MOCVD chamber. AlN film was directly grown on the graphene/NPSS without a low temperature buffer layer. The conditions were 1200 °C and a mixed gas atmosphere of 500 sccm NH₃ and 50 sccm trimethylaluminum (TMAI). Then, a 2 μm thick layer of Si-doped n-GaN, a nine-period layer of In_xGa_{1-x}N/GaN multiquantum-wells, and a 150 nm thick layer of Mg-doped p-GaN were deposited on the AlN/graphene/NPSS.

Characterization: The morphology and structure of the selectively grown graphene, AlN, and UV-LED structure on NPSS were characterized with SEM (Hitachi S-4800, operated at 1 kV), Raman spectroscopy (WITec, alpha300 RS, with laser spot size ≈500 nm), environment scanning electron microscopy (FEI Quanta 200F), AFM (BRUKER Dimension Icon), X-ray diffraction (Rigaku, D/MAX 2500 PC), TEM (FEI Tecnai F20, operated at 200 kV), and Aberration-corrected TEM (Nion U-HERMES 200, operated at 60 kV and FEI Titan Cubed Themis G2 300, operated at 300 kV).

Supporting Information

Supporting Information is available from the Wiley Online Library or from the author.

Acknowledgements

Z.C., H.C., and T.C. contributed equally to this work. This work was supported by the National Basic Research Program of China (Nos.

2016YFA0200103, 2018YFB0406703, and 2016YFA0300804), the National Natural Science Foundation of China (Nos. 51520105003, 61974139, 61527814, 61427901, 11974023, and 51672007), the Key R&D Program of Guangdong Province (2018B030327001 and 2018B010109009), the "2011 Program" Peking-Tsinghua-IOP Collaborative Innovation Center for Quantum Matter and Beijing Natural Science Foundation (No. 4182063) and the Institute for Basic Science (IBS-R019-D1), South Korea. The authors acknowledge Electron Microscopy Laboratory in Peking University for the use of Cs corrected electron microscope. The DFT calculations were carried out on TianHe-1(A) at National Supercomputer Center in Tianjin. The authors also acknowledge the usage of the IBS-CMCM high-performance computing system simulator and high-performance computing platform of Peking University.

Conflict of Interest

The authors declare no conflict of interest.

Keywords

chemical vapor deposition, dielectric substrates, direct growth, graphene, light emitting diodes

Received: February 16, 2020

Revised: April 27, 2020

Published online: June 11, 2020

- [1] A. K. Geim, K. S. Novoselov, *Nat. Mater.* **2007**, *6*, 183.
- [2] K. S. Novoselov, V. I. Fal'ko, L. Colombo, P. R. Gellert, M. G. Schwab, K. Kim, *Nature* **2012**, *490*, 192.
- [3] A. S. Mayorov, R. V. Gorbachev, S. V. Morozov, L. Britnell, R. Jalil, L. A. Ponomarenko, P. Blake, K. S. Novoselov, K. Watanabe, T. Taniguchi, A. K. Geim, *Nano Lett.* **2011**, *11*, 2396.
- [4] A. A. Balandin, *Nat. Mater.* **2011**, *10*, 569.
- [5] C. Lee, X. Wei, J. W. Kysar, J. Hone, *Science* **2008**, *321*, 385.
- [6] R. A. Nair, P. Blake, A. N. Grigorenko, K. S. Novoselov, T. J. Booth, T. Stauber, N. M. R. Peres, A. K. Geim, *Science* **2008**, *320*, 1308.
- [7] Y. Cao, V. Fatemi, A. Demir, S. Fang, S. L. Tomarken, J. Y. Luo, J. D. Sanchez-Yamagishi, K. Watanabe, T. Taniguchi, E. Kaxiras, R. C. Ashoori, P. Jarillo-Herrero, *Nature* **2018**, *556*, 80.
- [8] Y. Cao, V. Fatemi, S. Fang, K. Watanabe, T. Taniguchi, E. Kaxiras, P. Jarillo-Herrero, *Nature* **2018**, *556*, 43.
- [9] D. Liang, T. Wei, J. Wang, J. Li, *Nano Energy* **2020**, *69*, 104463.
- [10] Y. M. Lin, C. Dimitrakopoulos, K. A. Jenkins, D. B. Farmer, H. Y. Chiu, A. Grill, P. Avouris, *Science* **2010**, *327*, 662.
- [11] F. Bonaccorso, Z. Sun, T. Hasan, A. C. Ferrari, *Nat. Photonics* **2010**, *4*, 611.
- [12] M. D. Stoller, S. Park, Y. Zhu, J. An, R. S. Ruoff, *Nano Lett.* **2008**, *8*, 3498.
- [13] R. Yin, Z. Xu, M. Mei, Z. Chen, K. Wang, Y. Liu, T. Tang, M. K. Priyadarshi, X. Meng, S. Zhao, B. Deng, H. Peng, Z. Liu, X. Duan, *Nat. Commun.* **2018**, *9*, 2334.
- [14] A. Reina, X. Jia, J. Ho, D. Nezich, H. Son, V. Bulovic, M. S. Dresselhaus, J. Kong, *Nano Lett.* **2009**, *9*, 30.
- [15] X. Li, W. Cai, J. An, S. Kim, J. Nah, D. Yang, R. Piner, A. Velamakanni, I. Jung, E. Tutuc, S. K. Banerjee, L. Colombo, R. S. Ruoff, *Science* **2009**, *324*, 1312.
- [16] L. Gao, G.-X. Ni, Y. Liu, B. Liu, A. H. Castro Neto, K. P. Loh, *Nature* **2014**, *505*, 190.
- [17] Z. Zhang, J. Du, D. Zhang, H. Sun, L. Yin, L. Ma, J. Chen, D. Ma, H.-M. Cheng, W. Ren, *Nat. Commun.* **2017**, *8*, 14560.
- [18] W. Liu, B. L. Jackson, J. Zhu, C.-Q. Miao, C.-H. Chung, Y.-J. Park, K. Sun, J. Woo, Y.-H. Xie, *ACS Nano* **2010**, *4*, 3927.
- [19] Y. Zhou, K. P. Loh, *Adv. Mater.* **2010**, *22*, 3615.
- [20] C.-A. Di, D. Wei, G. Yu, Y. Liu, Y. Guo, D. Zhu, *Adv. Mater.* **2008**, *20*, 3289.
- [21] J. Chen, Y. Wen, Y. Guo, B. Wu, L. Huang, Y. Xue, D. Geng, D. Wang, G. Yu, Y. Liu, *J. Am. Chem. Soc.* **2011**, *133*, 17548.
- [22] J. Chen, Y. Guo, L. Jiang, Z. Xu, L. Huang, Y. Xue, D. Geng, B. Wu, W. Hu, G. Yu, Y. Liu, *Adv. Mater.* **2014**, *26*, 1348.
- [23] H. Ago, Y. Ito, N. Mizuta, K. Yoshida, B. Hu, C. M. Orofeo, M. Tsuji, K.-i. Ikeda, S. Mizuno, *ACS Nano* **2010**, *4*, 7407.
- [24] B. Hu, H. Ago, Y. Ito, K. Kawahara, M. Tsuji, E. Magome, K. Sumitani, N. Mizuta, K.-i. Ikeda, S. Mizuno, *Carbon* **2012**, *50*, 57.
- [25] X. H. Zeng, A. V. Pogrebnyakov, A. Kotcharov, J. E. Jones, X. X. Xi, E. M. Lysczek, J. M. Redwing, S. Y. Xu, J. Lettieri, D. G. Schlom, W. Tian, X. Q. Pan, Z. K. Liu, *Nat. Mater.* **2002**, *1*, 35.
- [26] K. Kaminaga, D. Oka, T. Hasegawa, T. Fukumura, *J. Am. Chem. Soc.* **2018**, *140*, 6754.
- [27] D. Sztienkiel, M. Foltyn, G. P. Mazur, R. Adhikari, K. Kosiel, K. Gas, M. Zgirski, R. Kruszka, R. Jakiela, T. Li, A. Piotrowska, A. Bonanni, M. Sawicki, T. Dietl, *Nat. Commun.* **2016**, *7*, 13232.
- [28] S. Nakamura, *Jpn. J. Appl. Phys.* **1991**, *30*, L170.
- [29] H. J. Song, M. Son, C. Park, H. Lim, M. P. Levendorf, A. W. Tsen, J. Park, H. C. Choi, *Nanoscale* **2012**, *4*, 3050.
- [30] M. A. Fanton, J. A. Robinson, C. Puls, Y. Liu, M. J. Hollander, B. E. Weiland, M. LaBella, K. Trumbull, R. Kasarda, C. Howsare, J. Stitt, D. W. Snyder, *ACS Nano* **2011**, *5*, 8062.
- [31] Z. Chen, X. Zhang, Z. Dou, T. Wei, Z. Liu, Y. Qi, H. Ci, Y. Wang, Y. Li, H. Chang, J. Yan, S. Yang, Y. Zhang, J. Wang, P. Gao, J. Li, Z. Liu, *Adv. Mater.* **2018**, *30*, 1801608.
- [32] H. Chang, Z. Chen, W. Li, J. Yan, R. Hou, S. Yang, Z. Liu, G. Yuan, J. Wang, J. Li, P. Gao, T. Wei, *Appl. Phys. Lett.* **2019**, *114*, 091107.
- [33] W. Wu, A. Katsnelson, O. G. Memis, H. Mohseni, *Nanotechnology* **2007**, *18*, 485302.
- [34] T. V. Cuong, H. S. Cheong, H. G. Kim, H. Y. Kim, C. H. Hong, E. K. Suh, H. K. Cho, B. H. Kong, *Appl. Phys. Lett.* **2007**, *90*, 131107.
- [35] I. Batyrev, A. Alavi, M. W. Finnis, *Faraday Discuss.* **1999**, *114*, 33.
- [36] A. Tougerti, C. Méthivier, S. Cristol, F. Tielens, M. Che, X. Carrier, *Phys. Chem. Chem. Phys.* **2011**, *13*, 6531.
- [37] B. Hou, R. Xiang, T. Inoue, E. Einarsson, S. Chiashi, J. Shiomi, A. Miyoshi, S. Maruyama, *Jpn. J. Appl. Phys.* **2011**, *50*, 065101.
- [38] L. Zhang, F. Xu, J. Wang, C. He, W. Guo, M. Wang, B. Sheng, L. Lu, Z. Qin, X. Wang, B. Shen, *Sci. Rep.* **2016**, *6*, 35934.
- [39] D. Lee, J. W. Lee, J. Jang, I. S. Shin, L. Jin, J. H. Park, J. Kim, J. Lee, H. S. Noh, Y. I. Kim, Y. Park, *Appl. Phys. Lett.* **2017**, *110*, 191103.